

## Article

# Development of Directional 14 MeV-Fusion Neutron Detector Using Liquid-Scintillator-Filled Capillaries

Masataka Teshigawara <sup>1,†</sup>, Eiji Takada <sup>2,\*</sup>, Shuhei Sumida <sup>3</sup>, Kouji Shinohara <sup>3,4</sup>, Takeo Nishitani <sup>5</sup>, Sangaroon Siriyaporn <sup>6</sup>, Longyong Liao <sup>7</sup>, Kunihiro Ogawa <sup>7,8</sup>, Mitsutaka Isobe <sup>7,8</sup>, Shigeo Matsuyama <sup>9</sup>, Misako Miwa <sup>9</sup>, Sho Toyama <sup>9</sup>, Isao Murata <sup>10</sup>, Shingo Tamaki <sup>10</sup> and Sachie Kusaka <sup>10</sup>

<sup>1</sup> National Institute of Technology, Toyama College, 13 Hongo-machi, Toyama 939-8630, Japan

<sup>2</sup> National Institute of Technology, Gakujutsu-Sogo-Center 10F, 2-1-1 Hitotsubashi, Chiyoda-ku 101-0003, Japan

<sup>3</sup> National Institutes for Quantum Science and Technology, 801-1 Mukoyama, Naka 311-0193, Japan; shinohara@k.u-tokyo.ac.jp (K.S.)

<sup>4</sup> Graduate School of Frontier Sciences, The University of Tokyo, 5-1-5 Kashiwanoha, Kashiwa 277-0882, Japan

<sup>5</sup> Graduate School of Engineering, Nagoya University, Furo-cho, Chikusa-ku, Nagoya 464-8601, Japan

<sup>6</sup> Department of Physics, Mahasarakham University, Maha Sarakham 44150, Thailand

<sup>7</sup> Fusion Science Program, The Graduate University for Advanced Studies, SOKENDAI, 322-6 Oroshi-cho, Toki 509-5202, Japan

<sup>8</sup> National Institute for Fusion Science, 322-6 Oroshi-cho, Toki 509-5202, Japan

<sup>9</sup> Quantum Science and Energy Engineering, Graduate School of Engineering, Tohoku University, Sendai 980-8579, Japan; sho.toyama.a3@tohoku.ac.jp (S.T.)

<sup>10</sup> Division of Sustainable Energy and Environmental Engineering, Graduate School of Engineering, Osaka University, Yamadaoka 2-1, Suita 565-0871, Japan; kusaka@see.eng.osaka-u.ac.jp (S.K.)

\* Correspondence: e\_takada@kosen-k.go.jp

† Present address: Materials Science and Engineering, Tokyo Institute of Technology, 2-12-1, Ookayama, Meguro-ku 152-8550, Japan.



**Citation:** Teshigawara, M.; Takada, E.; Sumida, S.; Shinohara, K.; Nishitani, T.; Siriyaporn, S.; Liao, L.; Ogawa, K.; Isobe, M.; Matsuyama, S.; et al. Development of Directional 14 MeV-Fusion Neutron Detector Using Liquid-Scintillator-Filled Capillaries. *Electronics* **2023**, *12*, 3219. <https://doi.org/10.3390/electronics12153219>

Academic Editor: Lucas Lamata

Received: 29 May 2023

Revised: 4 July 2023

Accepted: 13 July 2023

Published: 25 July 2023



**Copyright:** © 2023 by the authors. Licensee MDPI, Basel, Switzerland. This article is an open access article distributed under the terms and conditions of the Creative Commons Attribution (CC BY) license (<https://creativecommons.org/licenses/by/4.0/>).

**Abstract:** Triton burnup studies have been performed in fusion experimental devices to evaluate the confinement performance of 3.5 MeV alpha particles. For this purpose, the generation rate of deuterium-tritium (D-T)-born 14 MeV neutrons has been measured using a scintillating fiber detector. The directionality of this detector provides excellent selectivity for 14 MeV neutrons; however, the lack of a pulse–shape discrimination (PSD) capability limits high-energy gamma-ray reduction. In this study, we developed a new 14 MeV neutron detector with directionality that can discriminate neutrons and gamma rays based on the PSD technique by filling capillaries with a liquid scintillator. The performance of this detector was evaluated at the FNL (Tohoku University, Japan) and OKTAVIAN (Osaka University, Japan). The detector response was modeled using the particle and heavy ion transport code system (PHITS). The experimental and simulation results demonstrated that the detector has a directional response to fast neutrons and excellent PSD capability.

**Keywords:** 14 MeV neutron; liquid scintillator; pulse–shape discrimination; scintillating fiber

## 1. Introduction

The confinement of 3.5 MeV alpha particles produced by the deuterium-tritium (D-T) reaction is essential for commercializing fusion energy because they heat and sustain plasma through colliding with the plasma. Therefore, triton burnup studies have been performed [1–7], where the ratio of the D-T neutron generation rate to the D-D neutron generation rate in deuterium plasma has been used to evaluate the confinement performance of triton particles. Because the spatial and time scale of the motion of triton particles resembles those of alpha particles [8], the behavior of alpha particles can be estimated.

For this purpose, various types of D-T neutron detectors have been developed and operated in experimental fusion devices. For example, silicon diodes, which have a high-energy resolution, were used to measure D-T neutrons produced by 1 MeV tritons at

TFTR [9–11]. They successfully measured the time evolution of 14 MeV neutrons. However, this detector is susceptible to radiation damage. In recent years, there have been advancements in the development of 14 MeV neutron detectors using silicon carbide or diamond crystals [12–20]. These detectors are gaining attention due to their reduced susceptibility to temperature changes, light, and radiation. However, they are expensive and have a limited counting efficiency due to their size constraints. Scintillating fiber (Sci. Fi.) detectors, which use plastic scintillators processed into a fiber form, have been used to conduct the time-resolved D-T neutron measurements at TFTR, LHD, JT-60U, and KSTAR [21–31]. This detector offers a high-speed response, radiation resistance, and directional sensitivity to 14 MeV neutrons. However, one drawback of this detector is that it does not have a pulse-shape discrimination (PSD) capability. Therefore, it uses pulse height discrimination to distinguish between signals from D-T neutrons and those from background gamma rays and D-D neutrons, which exploits the fact that the pulse height of the scintillation light is proportional to the energy deposited by the excited particle. By setting an appropriate threshold for the pulse height value, low-energy gamma rays and D-T neutrons can be discriminated. However, the light output of organic scintillators, including Sci. Fi. detectors, for electrons has a greater per unit energy than that of ions. Therefore, 2–3 MeV neutrons, which collide with ions in the detector, are required to provide the same light output as a 1 MeV gamma ray. For instance, the pulse height of a 7.8 MeV gamma ray due to the neutron capture reaction of  $^{56}\text{Fe}$  in stainless steel is compatible with that of 14 MeV (D-T) neutrons. Therefore, the contamination of signals by high-energy gamma rays is inevitable when using pulse-height discrimination alone. Organic scintillators such as stilbene (solid) and EJ-301 (liquid) have also been used as a D-T neutron detector at LHD [22–33] and JT-60U [34,35]. They offer a high counting efficiency and possess a PSD capability, enabling the differentiation of pulses originating from interactions between neutrons and gamma rays. However, unlike Sci. Fi. detectors, stilbene is not directional to D-T neutrons due to the difficulty in fabricating a long shape. On the other hand, liquid scintillators provide shape flexibility through container adjustment. However, preventing the quenching caused by dissolved oxygen necessitates the creation of an oxygen-free environment using nitrogen gas, which presents challenges when it comes to sealing it within the container.

This study focused on neutron–gamma ray discrimination using the PSD method. Material, such as stilbenes and liquid scintillators, can discriminate between neutrons and gamma rays using the difference in the time constant of the pulse decay depending on the excited particle. Therefore, although their pulse height values are comparable, neutrons and gamma rays can be discriminated. By filling capillaries with a liquid scintillator, we developed a new concept of a 14 MeV neutron detector with both directionalities, like Sci. Fi. detectors, and neutron–gamma-ray-discrimination capability using the PSD technique to provide the precise experimental data needed to elucidate the physics of high-energy alpha particle confinement. The performance of the detector was demonstrated at FNL (Tohoku University, Japan) [36] and OKTAVIAN (Osaka University, Japan) [37]. In addition, the detector response was modeled using the particle and heavy ion transport code system [38]. The experimental and simulation results demonstrated that the detector has a directional response to fast neutrons and an outstanding PSD capability. We anticipate that this detector can be installed in an environment with a total neutron emission rate exceeding  $10^{16}$  neutrons/s, which corresponds to a neutron flux of  $\sim 10^{10} \text{ cm}^{-2} \text{ s}^{-1}$  at the torus hall in LHD [39], where the Sci. Fi. detectors are installed.

## 2. Materials and Methods

### 2.1. Sci. Fi. Detector

Sci. Fi. detectors were developed in the 1990s to measure 14 MeV neutrons for fusion experimental devices, such as TFTR and JT-60U. As shown in Figure 1, a Sci. Fi. detector consists of a sensor head with several scintillating fibers embedded in the housing, which is connected to a photomultiplier tube (PMT). The commonly used scintillating fiber in Sci. Fi. detectors is BCF-10 (Saint Gobain) [22,23,26]. Its emission peak is 432 nm, its decay time

is 2.7 ns, and its light yield is  $\sim$ 8000 photons/MeV (for a minimum ionizing particle (MIP), corrected for PMT sensitivity) [40]. The number of scintillating fibers to be embedded in the housing ranges from tens to hundreds depending on the application conditions. A neutron incident on a Sci. Fi. detector produces a recoil proton by elastic scattering with hydrogen atoms in the Sci. Fi. The recoil proton excites the electrons in the scintillator molecules; then, de-excitation leads to scintillation light emission, which the PMT detects.

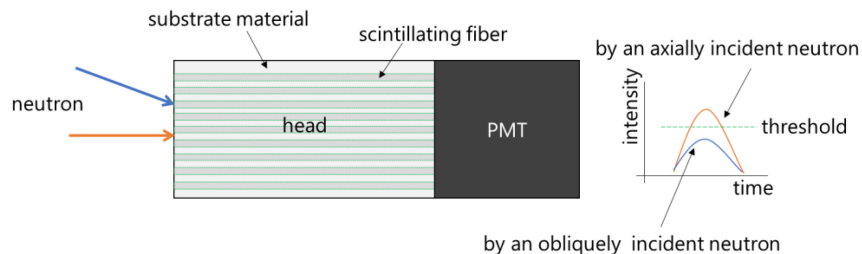


**Figure 1.** Structure of a Sci. Fi. detector. Pulse signals from an axially incident neutron (orange) and an obliquely incident neutron (blue).

The elongated shape of a Sci. Fi. allows axially recoiled protons to deposit all their energy to the scintillator; however, this is not the case for off-axis recoiled protons because the maximum range of the protons in the Sci. Fi. is shorter than the diameter of the Sci. Fi. The scattering angle of the recoil protons relative to the direction of neutron travel is close to  $0^\circ$ . Therefore, by setting an appropriate threshold, the Sci. Fi. detector can be used as a directional detector for 14 MeV neutrons.

## 2.2. Capillary-Filled Liquid Scintillation Detector

The detector developed in this study consists of 144 capillaries (50 mm long and 2.0 mm in diameter) in the housing filled with a liquid scintillator, which is coupled to the PMT via Pyrex glass (Figure 2). Depending on the exciting particle, the liquid scintillator has a different decay time constant for a scintillation pulse, which enables the PSD technique. In addition, this detector has directionality because of its long and narrow shape, which is similar to a Sci. Fi. detector.

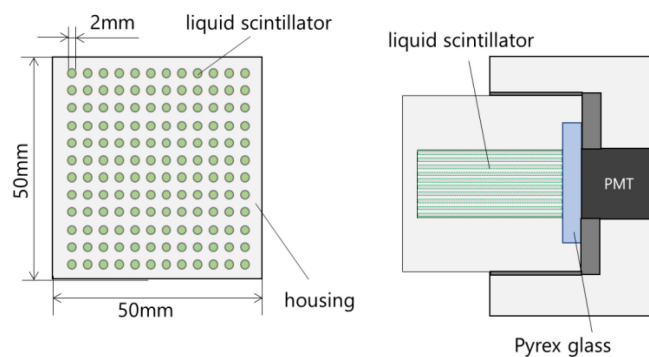


**Figure 2.** Structure of a capillary-filled liquid scintillation detector.

## 3. Experiments and Simulations

The liquid scintillator used was an EJ-301 device from Eljen Technology, and the PMT was an H111934-100 device from Hamamatsu. Conventionally, aluminum housing is used in Sci. Fi. detectors, and a previous study showed that multiple reflections from the housing attenuates the scintillation light, thus reducing the detection efficiency [28]. Therefore, in this study, a housing made of Teflon with better reflectivity was also fabricated to compare the detector responses. The anode signal from the PMT was fed directly into a digitizer (DT5751, CAEN). The charge integration method was used for the PSD, where two-time gates (short gate and long gate) were applied to the pulse, and the charges contained in

each gate were integrated ( $Q_{\text{short}}$  and  $Q_{\text{long}}$ ) with a 1 GHz sampling rate (Figure 3). This study fixed the short and long gates at 20 ns and 100 ns, respectively. The PSD parameter is defined as  $\text{PSD} = 1 - Q_{\text{short}}/Q_{\text{long}}$ .

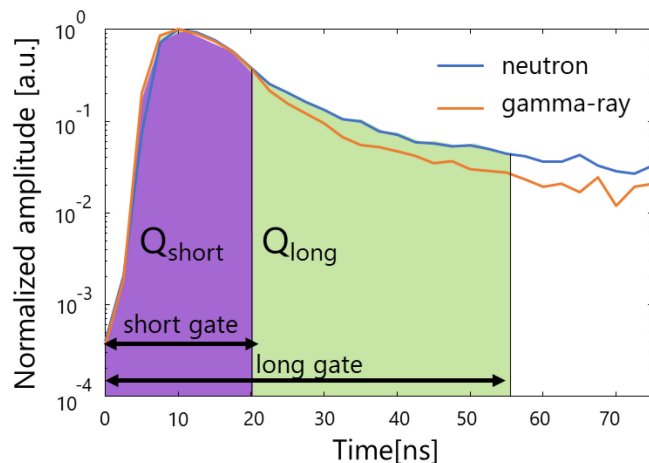


**Figure 3.** Definition of the short gate and long gate to calculate  $Q_{\text{short}}$  and  $Q_{\text{long}}$  in the charge integration method.

The directionality and PSD capability of the device were investigated in FNL at Tohoku University and OKTAVIAN at Osaka University. In FNL, a detector with an aluminum housing was used; in OKTAVIAN, a detector with a Teflon housing was used. In FNL, the accelerator produced deuterium-deuterium (D-D) and deuterium-lithium (D-Li) neutrons by irradiating a 3 MeV deuterium beam into a D<sub>2</sub> or Li target. The energies of the neutrons were ~6 and ~18 MeV, respectively. Their corresponding neutron rates at the target were about  $5.3 \times 10^6$  neutrons/s and  $1.6 \times 10^7$  neutrons/s. The distance from the target to the detector was 216 cm, and the angle between the target and the detector was zero degrees. The measurement time was set to 30 min. In OKTAVIAN, a deuterium beam of ~250 keV was injected into a tritium occlusion titanium target to produce D-T neutrons. The typical D-T neutron rate at the target was  $10^9$  neutrons/s. The measurement time was set to 10 min. The distance from the target to the detector was 77 cm, and the angle between the target and the detector was fifteen degrees.

To evaluate the directionality, the detector angle was varied from  $0^\circ$  to  $30^\circ$ ,  $45^\circ$ ,  $60^\circ$ , and  $90^\circ$  using a rotating table. Note that  $0^\circ$  was the direction in which neutrons were incident horizontally on the detector, and  $90^\circ$  was the direction in which neutrons were incident vertically on the detector. A <sup>137</sup>Cs gamma-ray source was used to evaluate the attenuation of the scintillation light. The experimental results were compared between the detectors with aluminum and Teflon housings. To simulate the response function of the detector with Teflon housing, SCINFUL-QMD [41], which is available in PHITS (particle and heavy ion transport code system, ver. 3.26) [38], was used. A <sup>252</sup>Cf neutron source was used to validate the simulation results.

#### 4. Results and Discussions

##### 4.1. Experimental Results with Fast Neutrons at FNL

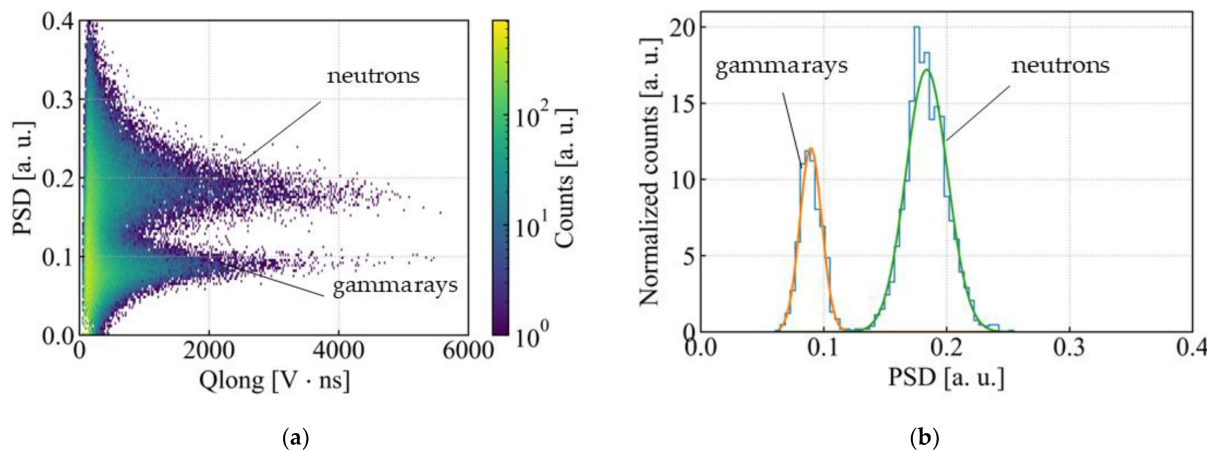
###### 4.1.1. PSD Capability

Figure 4a shows a 2D scatterplot based on  $Q_{\text{long}}$  and  $Q_{\text{short}}$  when the detector with aluminum housing was irradiated with D-D neutrons. As shown in Figure 4b, events due to gamma-rays and neutrons were discriminated by projecting from the 2D scatterplot in Figure 4 onto the PSD axis and fitting it with a mixed Gaussian distribution. The left and right peaks correspond to events caused by gamma rays and neutrons, respectively. Figure 5a shows a 2D scatterplot based on  $Q_{\text{long}}$  and  $Q_{\text{short}}$  when the detector with aluminum housing was irradiated with D-Li neutrons. Figure 5b shows the distribution of

PSD parameter. The higher energy of the neutrons, as compared to the D-D neutrons, led to a relatively lower number of events due to gamma rays above the threshold. To evaluate the discrimination performance in each distribution, an index of discrimination performance, the figure of merit (FoM), is defined as the following equation:

$$\text{FoM} = \frac{d}{\sigma_1 + \sigma_2}$$

where  $d$  is the distance between the peaks of each distribution, and the  $\sigma_1$  and  $\sigma_2$  are standard deviations. The FoM depended on the incident neutron energy;  $\text{FoM} = 3.7$  for D-D neutrons and  $\text{FoM} = 2.5$  for D-Li neutrons. Therefore, the optimal long gate and short gate should be selected according to the incident neutron energy.



**Figure 4.** (a) Two-dimensional scatter plots based on  $Q_{\text{short}}$  and  $Q_{\text{long}}$ . (b) Distribution of PSD parameters above  $Q_{\text{long}} 2000$ . D-D neutrons were irradiated to the detector with an aluminum housing.

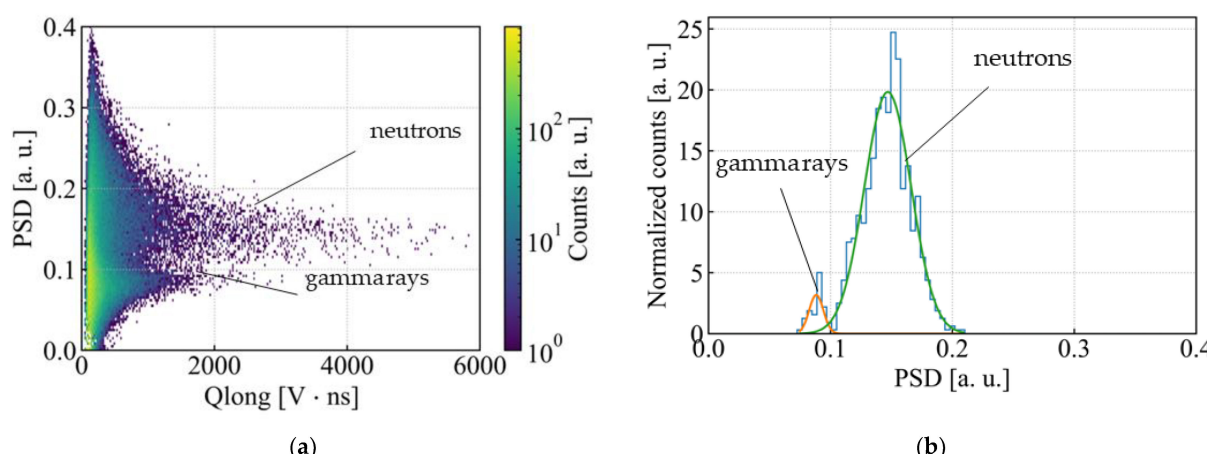
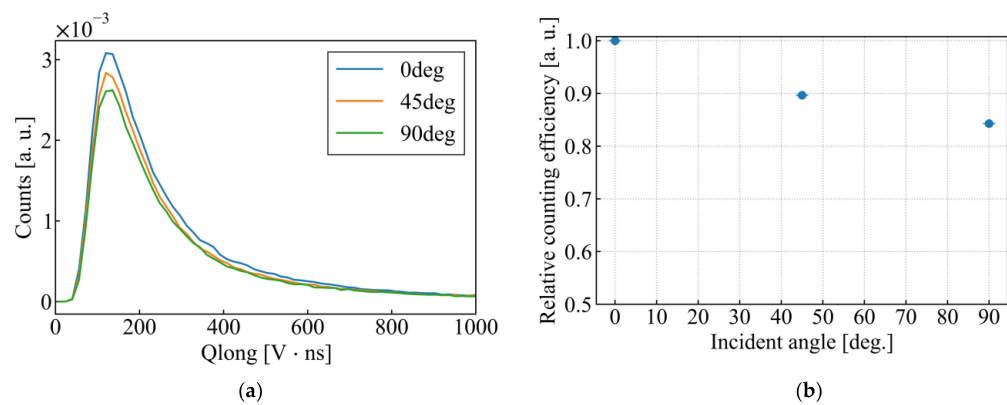


**Figure 5.** (a) Two-dimensional scatter plots based on  $Q_{\text{short}}$  and  $Q_{\text{long}}$ . (b) Distribution of PSD parameters above  $Q_{\text{long}} 2000$ . D-Li neutrons were irradiated to the detector with an aluminum housing.

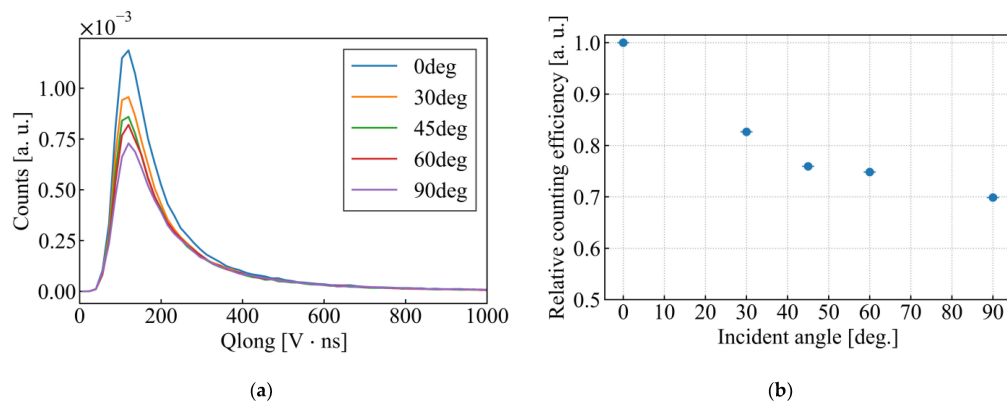
#### 4.1.2. Directionality

Figure 6a shows the dependence of the  $Q_{\text{long}}$  distribution on the incident angle for D-D neutrons. The total neutron rate normalized the number of counts based on  ${}^3\text{He}$  proportional counter measurements. Figure 6b shows the relative counting rate as a function of the detector angle around  $Q_{\text{long}} 100\text{--}400$ . Figure 7a shows the dependence of the  $Q_{\text{long}}$  distribution on the incident angle for D-Li neutrons. Figure 7b shows the relative counting rate as a function of the detector angle around  $Q_{\text{long}} 100\text{--}400$ . The larger the

detector angle, the smaller the count rate. Therefore, neutrons incident in the front direction could be selectively measured. In addition, the higher the incident energy of the neutrons, the greater the dependence on the incident angle because a longer distance was required for the recoil proton to deposit all of its energy. However, the full-width half-maximum of the relative counting rate was lower than that of the Sci. Fi. detector (20–40 deg) [24–26] because the capillary diameter of this detector (2 mm) was longer than that of the Sci. Fi. detector (typically, 1 mm), and the scintillation light generated by axially incident neutrons was significantly attenuated to reduce the detection efficiency, thereby deteriorating the directionality. Furthermore, in ref. [24–26], the Sci. Fi. detector showed a dependence on the incident angle in the high-energy region. However, our detector demonstrated this in the low-energy region. Because the pulse height value decreased with the scintillation light attenuation, the overall response spectrum shifted to the lower-energy side. The effects of scintillation photon attenuation are discussed in detail in Section 4.2.



**Figure 6.** (a) Dependence of  $Q_{\text{long}}$  distribution on incident angle. (b) The relative counting rate as a function of the detector angle around  $Q_{\text{long}}$  100–400. D-D neutrons were irradiated to the detector with aluminum housing. The counting rate was normalized by the total neutron rate based on  ${}^3\text{He}$  proportional counter measurements.



**Figure 7.** (a) Dependence of  $Q_{\text{long}}$  distribution on incident angle. (b) The relative counting rate as a function of the detector angle around  $Q_{\text{long}}$  100–400. D-Li neutrons were irradiated to the detector with aluminum housing. The counting rate was normalized by the total neutron rate based on  ${}^3\text{He}$  proportional counter measurements.

#### 4.2. Experimental Results on Attenuation of Scintillation Photons with a ${}^{137}\text{Cs}$ Gamma-Ray Source

The scintillation light generated in the liquid scintillator propagated to the photocathode of the PMT through multiple reflections with the housing. For example, the scintillation light generated at a longer distance from the photocathode was expected to have a greater attenuation owing to the increased number of reflections. However, the scintillation light

generated closer to the photocathode was anticipated to be almost unattenuated. Therefore, even if the scintillation light originally had the same emission amount, the detectable amount differed depending on its generated position. This effect was more pronounced when the neutrons were axially incident because the number of scintillation events in the front part of the detector was relatively greater than when they were vertically incident.

The attenuation of scintillation light as a function of the generated position was investigated using a  $^{137}\text{Cs}$  gamma-ray source. Figure 8 illustrates the experimental configuration. The gamma rays were collimated with a lead block and injected perpendicular to the detector while gradually shifting the incident position by 5 mm. This experiment was conducted for the detectors constructed with an aluminum housing and a Teflon housing and with a Sci. Fi. detector. Gamma rays were irradiated using a collimator with a 5 mm diameter to ensure a sufficient counting rate.

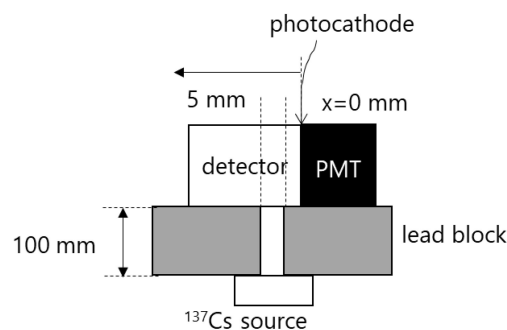


**Figure 8.** Experimental setup to investigate the relationship between the generation position of scintillation light and its attenuation.

Figure 9a,b show the  $Q_{\text{long}}$  distribution as a function of incident position of the gamma rays. Figure 10 also shows the dependence of the relative counting efficiency on the incident position for events with  $Q_{\text{long}} > 60\%$  of the maximum value. The liquid scintillation detector with the Teflon housing had a relatively low attenuation because its white color had a high reflectivity. The counting efficiency of the liquid scintillation detector with the aluminum housing became close to 0 at 15 mm or more from the photocathode, which means that the scintillation light generated at the entrance region of the detector was almost undetectable. This was because the low reflectivity of the aluminum housing greatly attenuated the scintillation photons.

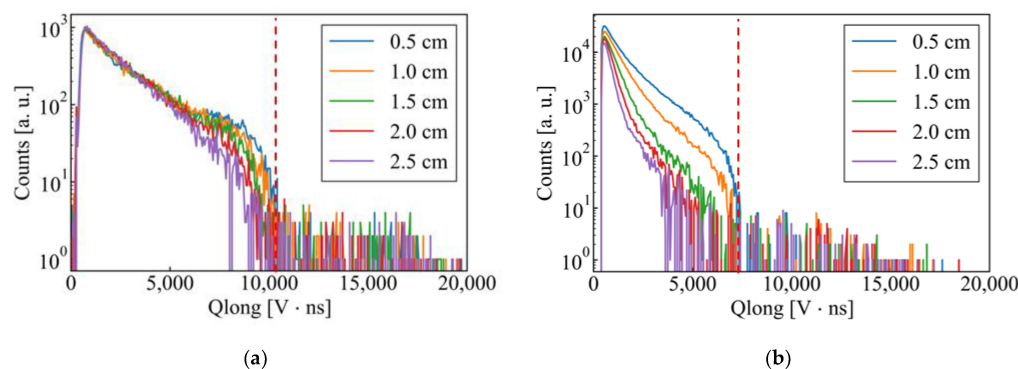


**Figure 9.** (a)  $Q_{\text{long}}$  distribution for the liquid scintillation detector with the Teflon housing as a function of gamma ray incident position. The measurement time was 600 s. (b)  $Q_{\text{long}}$  distribution for the liquid scintillation detector with the Al housing as a function of gamma ray incident position. The measurement time was 18,000 s.

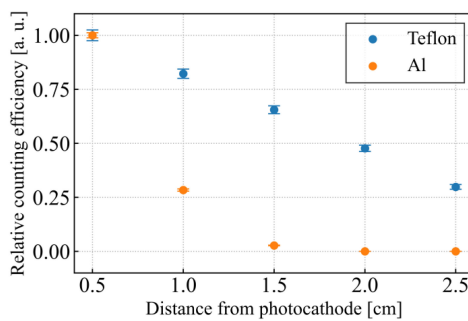


**Figure 10.** Comparison of counting efficiencies of the aluminum housing and Teflon housing as a function of gamma ray incident position. The counting efficiency was normalized based on an incident position of 0.5 cm from the photocathode. The threshold of  $Q_{\text{long}}$  was 60% of the maximum  $Q_{\text{long}}$  value (red dashed line in Figure 9a,b) for each distribution.

#### 4.3. Experimental Results with 14 MeV Neutrons at OKTAVIAN

Figure 11a shows the dependence of the  $Q_{\text{long}}$  distribution on the incident angle when D-T neutrons were irradiated to the detector with Teflon housing. Figure 11b shows the relative counting rate as a function of the detector angle for  $Q_{\text{long}} \geq 30,000$ . Like the Sci. Fi. detector, dependence on the incident angle was observed in the high-energy region. The increase in counts at  $90^\circ$  was likely due to errors in the position and angle. The FWHM was approximately  $40^\circ$ , which was better than that of the detector with the aluminum housing. The Teflon housing improved the collection efficiency of the scintillation light, which led to a better directionality than the detector with the aluminum housing. The detector with the aluminum housing showed an angular dependence at the lower-energy part due to the attenuation of scintillation photons; because the range to integrate  $Q_{\text{long}}$  needed to be set at a the lower-energy part, the directionality was deteriorated by background gamma rays and low-energy neutrons. On the other hand, the detector with the Teflon housing showed an angular dependence in the high-energy part, which allowed a higher  $Q_{\text{long}}$  range, thus improving the directionality. The knee-like distribution of  $Q_{\text{long}}$  from 10,000 to 25,000 corresponded to the protons recoiled by the D-T neutrons depositing all of their energy into the liquid scintillator. The response spectrum shifted to the lower-energy side as the incident angle increased. This shift means that this detector was directional to D-T neutrons. The tail-like distribution of  $Q_{\text{long}}$  above 25,000 was formed by events generated in the liquid scintillator pool near the photocathode. Because reflections from the housing did not attenuate the scintillation light generated in the liquid scintillation pool, it was efficiently collected, which caused a larger  $Q_{\text{long}}$ .

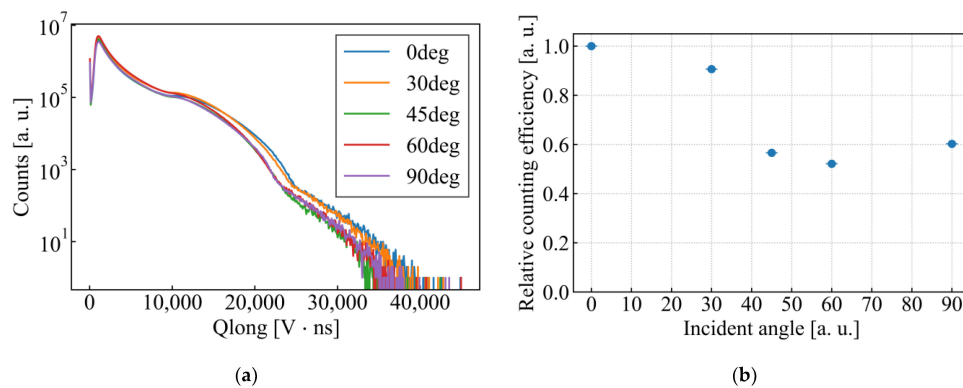


**Figure 11.** (a) Dependence of  $Q_{\text{long}}$  distribution on incident angle. (b) The relative counting rate as a function of the detector angle with  $Q_{\text{long}} \geq 20,000$ . D-T neutrons were irradiated to the detector with Teflon housing. The counting rate was normalized by the total neutron rate based on  ${}^3\text{He}$  proportional counter measurements.

#### 4.4. Comparison between Experimental and Simulation Results

In SCINFUL-QMD, the nuclear reaction between neutrons and carbon nuclei in a cell defined as an organic scintillator was calculated in the SCINFUL mode, and the energy deposited by the generated charged particles was converted to a light output to create a response function. In ref. [28], the authors simulated the detector response of a Sci. Fi. detector using PHITS by considering that the generation efficiency of scintillation photons depends on the excited particle. However, to precisely replicate the detector response, the attenuation of scintillation light should also be considered. SCINFUL-QMD was calculated based on the following equation:

$$L = L' \cdot \exp(-G \cdot D) \quad (1)$$

where  $L'$  (MeVee) and  $L$  (MeVee) are the electron-equivalent energy deposition before and after attenuation, respectively.  $G$  is the attenuation coefficient ( $\text{cm}^{-1}$ ), and  $D$  (cm) is the distance from the generation position of the scintillation light to the photocathode position. The statistical variation in the light output was assumed to be a Gaussian distribution, and the following equation was used to define its standard deviation:

$$U = \sqrt{\sigma^2 + F \cdot L} \quad (2)$$

where  $\sigma$  represents system-specific variations, such as electrical noise. In addition,  $F \cdot L$  expresses the variation in the optical output according to the Poisson distribution, where  $F$  denotes the proportional coefficient when the number of generated photons is assumed to be proportional to  $L$ . The simulated light output should be digitized for comparison with the experimental results. This was performed using the following equation [42]:

$$Q_{\text{long}} = \frac{N \cdot QE \cdot \text{pmt\_gain} \cdot e}{\text{digitizer\_charge\_sensitivity}} \quad (3)$$

In this study, the digitizer's charge sensitivity was set to  $20 \times 10^{-15} \text{ C/LSB}$ . The PMT gain was  $2.0 \times 10^5$ , and the quantum efficiency (QE) was 0.35 [43]. The number of generated photons ( $N$ ) was obtained as  $N = \text{scintillation\_yield} \times L$ , where the scintillation yield of EJ-301 was 12,000 photons/MeVee [44]. The charge of an electron ( $e$ ) is  $1.6022 \times 10^{-19} \text{ C}$ . Substituting these, the following equation can be obtained:

$$Q_{\text{long}} = 6728.4 \times L \quad (4)$$

A geometrical model identical to the actual detector with the Teflon housing was created, and the detector was irradiated with neutrons emitted from a  $^{252}\text{Cf}$  neutron source. Figure 12 shows the simulation and experimental results. By adjusting the attenuation coefficient,  $G$ , of the scintillation light while fixing the other variables, we reproduced a  $Q_{\text{long}}$  distribution similar to the experimental results. In the experiment, the number of counts in the low-energy part was lower than in the simulation results because of the threshold value required to remove background and noise. The response spectrum shifted to higher energies with smaller attenuation coefficients owing to the increased collection efficiency of the scintillation light. The prospect that the experimental results can be reproduced by simulation was obtained, and it is now possible to optimize the detector geometry based on the simulation results.

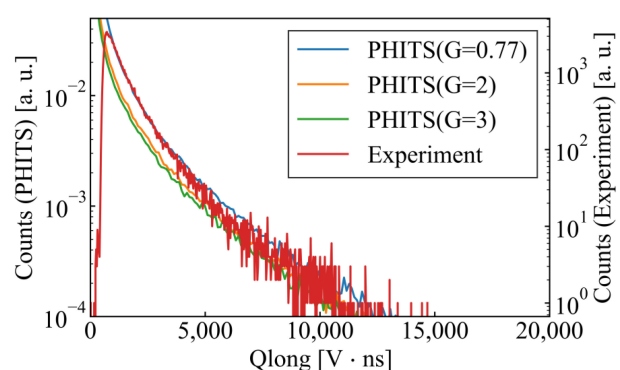


**Figure 12.** Comparison of  $Q_{\text{long}}$  distributions obtained from simulation and experimental results.

## 5. Conclusions

A capillary-filled liquid scintillation detector was developed for triton burnup studies. This detector comes in two variations, utilizing either aluminum or Teflon housings. Through fast neutron irradiation experiments using an accelerator, it was demonstrated that this detector possessed an excellent PSD capability and directionality. The figure of merit for D-D neutrons was determined to be 3.7, while for D-Li neutrons, it was 2.5. Furthermore, the detector with the Teflon housing exhibited an angular resolution of approximately  $40^\circ$  for D-T neutrons. Additionally, the experiments conducted with a  $^{137}\text{Cs}$  gamma ray source indicated that the Teflon housing exhibited lower scintillation light attenuation compared to the aluminum housing. This suggests that the use of Teflon housing could contribute to an improved directionality, which led to an improvement in the angular resolution. To validate the results obtained with the Teflon housing, the detector's response was reproduced using PHITS, a particle transport simulation code. This simulation opened the possibility of optimizing the detector's geometry based on these replicated experimental results. By employing the PSD method after discriminating between low-energy neutrons and gamma rays based on directionality, more accurate measurements of 14 MeV neutrons in triton burnup studies can be achieved. The effectiveness and applicability of this detector will be further investigated through measurements of secondary D-T neutrons at LHD.

**Author Contributions:** Conceptualization, E.T., S.S. (Shuhei Sumida), K.S., T.N., K.O. and M.I.; Methodology, E.T., K.S., T.N., K.O. and M.I.; Software, M.T.; Validation, E.T. and S.S. (Shuhei Sumida); Formal analysis, M.T.; Resources, S.M., M.M., S.T. (Sho Toyama), I.M., S.T. (Shingo Tamaki) and S.K.; Data curation, M.T., S.S. (Sangaroon Siriyaporn) and L.L.; Writing—original draft, M.T.; Writing—review & editing, E.T., S.S. (Shuhei Sumida), T.N., K.O. and M.I.; Visualization, M.T.; Supervision, E.T., K.S., K.O. and M.I.; Project administration, E.T. and M.I.; Funding acquisition, E.T., K.O. and M.I. All authors have read and agreed to the published version of the manuscript.

**Funding:** This work was performed with the support and under the auspices of the NIFS Collaboration Research program (NIFS20KLEH085, NIFS22KIPH003, NIFS23KIPH025).

**Data Availability Statement:** The data presented in this study are available on request from the corresponding author.

**Conflicts of Interest:** The authors declare no conflict of interest.

## References

- Nishitani, T.; Hoek, M.; Harano, H.; Isobe, M.; Tobita, K.; Kusama, Y.; Wurden, G.; Chrien, R. Triton burnup study in JT-60U. *Plasma Phys. Control. Fusion* **1996**, *38*, 355. [[CrossRef](#)]
- Jo, J.; Cheon, M.; Kim, J.Y.; Rhee, T.; Kim, J.; Shi, Y.-J.; Isobe, M.; Ogawa, K.; Chung, K.-J.; Hwang, Y. Triton burnup measurements in KSTAR using a neutron activation system. *Rev. Sci. Instrum.* **2016**, *87*, 11D828. [[CrossRef](#)] [[PubMed](#)]
- Isobe, M.; Ogawa, K.; Nishitani, T.; Miyake, H.; Kobuchi, T.; Pu, N.; Kawase, H.; Takada, E.; Tanaka, T.; Li, S. Neutron diagnostics in the large helical device. *IEEE Trans. Plasma Sci.* **2018**, *46*, 2050–2058. [[CrossRef](#)]
- Pu, N.; Nishitani, T.; Ogawa, K.; Isobe, M.; Murakami, S.; Group, L.E. Initial results of triton burnup study in the large helical device. *Plasma Fusion Res.* **2018**, *13*, 3402121. [[CrossRef](#)]

5. Ogawa, K.; Isobe, M.; Nishitani, T.; Murakami, S.; Seki, R.; Nakata, M.; Takada, E.; Kawase, H.; Pu, N.; Group, L.E. Time-resolved triton burnup measurement using the scintillating fiber detector in the large helical device. *Nucl. Fusion* **2018**, *58*, 034002. [[CrossRef](#)]
6. Ogawa, K.; Isobe, M.; Nishitani, T.; Murakami, S.; Seki, R.; Nuga, H.; Kamio, S.; Fujiwara, Y.; Yamaguchi, H.; Saito, Y. Energetic ion confinement studies using comprehensive neutron diagnostics in the Large Helical Device. *Nucl. Fusion* **2019**, *59*, 076017. [[CrossRef](#)]
7. Ogawa, K.; Isobe, M.; Osakabe, M. Progress on integrated neutron diagnostics for deuterium plasma experiments and energetic particle confinement studies in the Large Helical Device during the campaigns from FY2017 to FY2019. *Plasma Fusion Res.* **2021**, *16*, 110203. [[CrossRef](#)]
8. Heidbrink, W.W.; Sadler, G.J. The behaviour of fast ions in tokamak experiments. *Nucl. Fusion* **1994**, *34*, 535. [[CrossRef](#)]
9. Bosch, H.S.; Strachan, J.; Barnes, C.W.; Nieschmidt, E. Calibration of a surface barrier detector for 14-MeV neutron flux measurements on TFTR. *Rev. Sci. Instrum.* **1988**, *59*, 1718–1720. [[CrossRef](#)]
10. Johnson, L.; Barnes, C.W.; Duong, H.; Heidbrink, W.; Jassby, D.; Loughlin, M.; Roquemore, A.; Ruskov, E.; Strachan, J. Cross calibration of neutron detectors for deuterium-tritium operation in TFTR. *Rev. Sci. Instrum.* **1995**, *66*, 894–896. [[CrossRef](#)]
11. Ruskov, E.; Heidbrink, W.; Duong, H.; Roquemore, A.; Strachan, J. Measurement of 14 MeV neutrons at TFTR with Si-diode detectors. *Rev. Sci. Instrum.* **1995**, *66*, 910–912. [[CrossRef](#)]
12. Flammang, R.W.; Seidel, J.G.; Ruddy, F.H. Fast neutron detection with silicon carbide semiconductor radiation detectors. *Nucl. Instrum. Methods Phys. Res. Sect. A Accel. Spectrom. Detect. Assoc. Equip.* **2007**, *579*, 177–179. [[CrossRef](#)]
13. Angelone, M.; Lattanzi, D.; Pillon, M.; Marinelli, M.; Milani, E.; Tucciarone, A.; Verona-Rinati, G.; Popovichev, S.; Montereali, R.; Vincenti, M. Development of single crystal diamond neutron detectors and test at JET tokamak. *Nucl. Instrum. Methods Phys. Res. Sect. A Accel. Spectrom. Detect. Assoc. Equip.* **2008**, *595*, 616–622. [[CrossRef](#)]
14. Liu, L.; Liu, A.; Bai, S.; Lv, L.; Jin, P.; Ouyang, X. Radiation resistance of silicon carbide Schottky diode detectors in DT fusion neutron detection. *Sci. Rep.* **2017**, *7*, 13376. [[CrossRef](#)]
15. Obraztsova, O.; Ottaviani, L.; Klix, A.; Döring, T.; Palais, O.; Lyoussi, A. Comparing the response of a SiC and a sCVD diamond detectors to 14-MeV neutron radiation. *IEEE Trans. Nucl. Sci.* **2018**, *65*, 2380–2384. [[CrossRef](#)]
16. Rebai, M.; Rigamonti, D.; Cancelli, S.; Croci, G.; Gorini, G.; Cippo, E.P.; Putignano, O.; Tardocchi, M.; Altana, C.; Angelone, M. New thick silicon carbide detectors: Response to 14 MeV neutrons and comparison with single-crystal diamonds. *Nucl. Instrum. Methods Phys. Res. Sect. A Accel. Spectrometers Detect. Assoc. Equip.* **2019**, *946*, 162637. [[CrossRef](#)]
17. Schmid, G.; Koch, J.; Lerche, R.; Moran, M. A neutron sensor based on single crystal CVD diamond. *Nucl. Instrum. Methods Phys. Res. Sect. A Accel. Spectrom. Detect. Assoc. Equip.* **2004**, *527*, 554–561. [[CrossRef](#)]
18. Xu, P.; Yu, Y.; Zhou, H. Fabrication of single-crystal diamond neutron detector and its application in 14.1 MeV neutron detection in deuteriumtritium fusion experiment. *Plasma Sci. Technol.* **2023**, *25*, 075101. [[CrossRef](#)]
19. Ogawa, K.; Isobe, M.; Weiss, C.; Griesmayer, E.; Sangaroon, S.; Takada, E.; Masuzaki, S.; Ohtani, H.; Liao, L.; Tamaki, S. Fusion product diagnostics based on commercially available chemical vapor deposition diamond detector in large helical device. *J. Instrum.* **2023**, *18*, P01022. [[CrossRef](#)]
20. Kobayashi, M.I.; Yoshihashi, S.; Ogawa, K.; Isobe, M.; Miwa, M.; Toyama, S.; Matsuyama, S.; Osakabe, M. Measurement of 6Li burn-up reaction rate using a single crystal CVD diamond detector under fast neutron irradiation environment. *Fusion Eng. Des.* **2023**, *193*, 113799. [[CrossRef](#)]
21. Sailor, W.; Barnes, C.W.; Chrien, R.; Wurden, G. Conceptual design for a scintillating-fiber neutron detector for fusion reactor plasma diagnostics. *Rev. Sci. Instrum.* **1995**, *66*, 898–900. [[CrossRef](#)]
22. Wurden, G.; Chrien, R.; Barnes, C.W.; Sailor, W.; Roquemore, A.; Lavelle, M.; O'gara, P.; Jordan, R. Scintillating-fiber 14 MeV neutron detector on TFTR during DT operation. *Rev. Sci. Instrum.* **1995**, *66*, 901–903. [[CrossRef](#)]
23. Nishitani, T.; Isobe, M.; Wurden, G.; Chrien, R.; Harano, H.; Tobita, K.; Kusama, Y. Triton burnup measurements using scintillating fiber detectors on JT-60U. *Fusion Eng. Des.* **1997**, *34*, 563–566. [[CrossRef](#)]
24. Ogawa, K.; Isobe, M.; Nishitani, T.; Takada, E.; Kawase, H.; Amitani, T.; Pu, N.; Jo, J.; Cheon, M.; Kim, J. High detection efficiency scintillating fiber detector for time-resolved measurement of triton burnup 14 MeV neutron in deuterium plasma experiment. *Rev. Sci. Instrum.* **2018**, *89*, 10I101. [[CrossRef](#)] [[PubMed](#)]
25. Takada, E.; Fujisaki, A.; Nakada, N.; Isobe, M.; Ogawa, K.; Nishitani, T.; Tomita, H. Development of fast-neutron directional detector for fusion neutron profile monitor at LHD. *Plasma Fusion Res.* **2016**, *11*, 2405020. [[CrossRef](#)]
26. Ogawa, K.; Isobe, M.; Sangaroon, S.; Takada, E.; Nakada, T.; Murakami, S.; Jo, J.; Zhong, G.; Zhang, Y.; Tamaki, S. Time-resolved secondary triton burnup 14 MeV neutron measurement by a new scintillating fiber detector in middle total neutron emission ranges in deuterium large helical device plasma experiments. *AAPPS Bull.* **2021**, *31*, 20. [[CrossRef](#)]
27. Pu, N.; Nishitani, T.; Ogawa, K.; Isobe, M. Scintillating fiber detectors for time evolution measurement of the triton burnup on the Large Helical Device. *Rev. Sci. Instrum.* **2018**, *89*, 10I105. [[CrossRef](#)]
28. Takada, E.; Amitani, T.; Fujisaki, A.; Ogawa, K.; Nishitani, T.; Isobe, M.; Jo, J.; Matsuyama, S.; Miwa, M.; Murata, I. Design optimization of a fast-neutron detector with scintillating fibers for triton burnup experiments at fusion experimental devices. *Rev. Sci. Instrum.* **2019**, *90*, 043503. [[CrossRef](#)]
29. Isobe, M.; Ogawa, K.; Sangaroon, S.; Kamio, S.; Fujiwara, Y.; Osakabe, M. Recent development of neutron and energetic-particle diagnostics for LHD deuterium discharges. *J. Instrum.* **2022**, *17*, C03036. [[CrossRef](#)]

30. Ogawa, K.; Isobe, M.; Kamio, S.; Nuga, H.; Seki, R.; Sangaroon, S.; Yamaguchi, H.; Fujiwara, Y.; Takada, E.; Murakami, S. Studies of energetic particle transport induced by multiple Alfvén eigenmodes using neutron and escaping energetic particle diagnostics in Large Helical Device deuterium plasmas. *Nucl. Fusion* **2022**, *62*, 112001. [[CrossRef](#)]
31. Lee, S.; Nam, Y.; Bak, J.; Juhn, J.; Lee, J.; Lee, K.; Seo, S.; Ko, W.; Ko, J.; Lee, J. Overview and recent progress of KSTAR diagnostics. *J. Instrum.* **2022**, *17*, C01065. [[CrossRef](#)]
32. Kawase, H.; Ogawa, K.; Nishitani, T.; Pu, N.; Isobe, M.; Group, L.E. Evaluation of spatial resolution of neutron profile monitor in LHD. *IEEE Trans. Plasma Sci.* **2018**, *47*, 462–465. [[CrossRef](#)]
33. Isobe, M.; Ogawa, K.; Sangaroon, S.; Zhong, G.; Fan, T. Recent Progress of Neutron Spectrometer Development for LHD Deuterium Plasmas. *Plasma Fusion Res.* **2022**, *17*, 2402008. [[CrossRef](#)]
34. Ishikawa, M.; Nishitani, T.; Morioka, A.; Takechi, M.; Shinohara, K.; Shimada, M.; Miura, Y.; Nagami, M.; Kaschuck, Y.A. First measurement of neutron emission profile on JT-60U using Stilbene neutron detector with neutron-gamma discrimination. *Rev. Sci. Instrum.* **2002**, *73*, 4237–4242. [[CrossRef](#)]
35. Itoga, T.; Ishikawa, M.; Baba, M.; Okuji, T.; Oishi, T.; Nakhostin, M.; Nishitani, T. Fast response neutron emission monitor for fusion reactor using stilbene scintillator and flash-ADC. *Radiat. Prot. Dosim.* **2007**, *126*, 380–383. [[CrossRef](#)]
36. Baba, M.; Takada, M.; Iwasaki, T.; Matsuyama, S.; Nakamura, T.; Ohguchi, H.; Nakao, T.; Sanami, T.; Hirakawa, N. Development of monoenergetic neutron calibration fields between 8 keV and 15 MeV. *Nucl. Instrum. Methods Phys. Res. Sect. A Accel. Spectrom. Detect. Assoc. Equip.* **1996**, *376*, 115–123. [[CrossRef](#)]
37. Schmid, G.; Koch, J.; Lerche, R.; Moran, M. Status of OKTAVIAN I and proposal for OKTAVIAN II. *Nucl. Sci. Eng.* **1990**, *106*, 249–265.
38. Sato, T.; Iwamoto, Y.; Hashimoto, S.; Ogawa, T.; Furuta, T.; Abe, S.-i.; Kai, T.; Tsai, P.-E.; Matsuda, N.; Iwase, H. Features of particle and heavy ion transport code system (PHITS) version 3.02. *J. Nucl. Sci. Technol.* **2018**, *55*, 684–690. [[CrossRef](#)]
39. Nishitani, T.; Ogawa, K.; Nishimura, K.; Isobe, M. Radiation field estimation for the diagnostic and control components by Monte Carlo neutronics calculations with LHD 3-dimensional modeling. *Plasma Fusion Res.* **2016**, *11*, 2405057. [[CrossRef](#)]
40. Sain, G. Available online: <https://www.crystals.saint-gobain.com/radiation-detection-scintillators/fibers> (accessed on 3 July 2023).
41. Satoh, D.; Sato, T. Improvements in the particle and heavy-ion transport code system (PHITS) for simulating neutron-response functions and detection efficiencies of a liquid organic scintillator. *J. Nucl. Sci. Technol.* **2022**, *59*, 1047–1060. [[CrossRef](#)]
42. Das, S.; Kashyap, V.K.S.; Mohanty, B. Energy calibration of EJ-301 scintillation detector using unfolding methods for fast neutron measurement. *Nucl. Instrum. Methods Phys. Res. Sect. A Accel. Spectrom. Detect. Assoc. Equip.* **2022**, *1042*, 167405. [[CrossRef](#)]
43. Hamamatsu. Available online: [https://www.hamamatsu.com/content/dam/hamamatsu-photronics/sites/documents/99\\_SALES\\_LIBRARY/etd/R11265U\\_H11934 TPMH1336E.pdf](https://www.hamamatsu.com/content/dam/hamamatsu-photronics/sites/documents/99_SALES_LIBRARY/etd/R11265U_H11934 TPMH1336E.pdf) (accessed on 2 July 2023).
44. Eljen Technology. Available online: <https://eljentechnology.com/products/liquid-scintillators/ej-301-ej-309> (accessed on 2 July 2023).

**Disclaimer/Publisher’s Note:** The statements, opinions and data contained in all publications are solely those of the individual author(s) and contributor(s) and not of MDPI and/or the editor(s). MDPI and/or the editor(s) disclaim responsibility for any injury to people or property resulting from any ideas, methods, instructions or products referred to in the content.